Asynchronous oscillations of rigid rods drive viscous fluid to swirl

Rintaro Hayashi and Daisuke Takagi

Phys. Rev. Fluids **2**, 124101 — Published 8 December 2017

DOI: 10.1103/PhysRevFluids.2.124101

Asynchronous Oscillations of Rigid Rods Drive Viscous Fluid to Swirl

Rintaro Hayashi

Department of Mechanical Engineering,

University of Hawai'i at Manoa, Honolulu, HI 96822, USA

Daisuke Takagi

Department of Mathematics, University of Hawai'i at Manoa, Honolulu, HI 96822, USA

Abstract

We present a minimal system for generating flow at low Reynolds number by oscillating a pair of rigid rods in silicone oil. Experiments show that oscillating them in phase produces no net flow, but a phase difference alone can generate rich flow fields. Tracer particles follow complex trajectory patterns consisting of small orbital movements every cycle and then drifting or swirling in larger regions after many cycles. Observations are consistent with simulations performed using the method of regularized Stokeslets, which reveal complex 3D flow structures emerging from simple oscillatory actuation. Our findings reveal the basic underlying flow structure around oscillatory protrusions such as hairs and legs as commonly featured on living and non-living bodies.

I. INTRODUCTION

The reversibility of viscous flow was elegantly demonstrated by G. I. Taylor in a fluid confined between two concentric cylinders: a small colored dye in the fluid gets sheared as the inner cylinder rotates slowly, and then remarkably returns to its original position after reversing the rotation [1]. No net flow arises from such a sequence of reciprocal motion at low Reynolds number (Re), a regime where viscosity dominates over inertia [2]. To generate flow with periodic motion, microorganisms typically employ flexible structures that can oscillate back and forth [3, 4], but rigid structures can also generate flows which are yet to be fully explored. The basic physical principle of driving flow with oscillatory motion has important implications on biophysics at small scales [5] and recent advances in micro- and nano-scale technology [6].

Here we demonstrate that oscillating a pair of rigid rods can generate rich flow fields consisting of numerous eddies, hereafter referred to as swirls. Table-top experiments confirm that a phase difference alone is sufficient for generating flow and they reveal qualitatively different flow patterns depending on the orientation of the rods. The experiments are complemented by simulations based on the method of regularized Stokeslets [7], which show that complex 3D flow structures arise from simple oscillatory actuation. Each oscillatory rod undergoes reciprocal motion, unlike the rotary motion of rigid bodies considered before [8]. The key driving mechanism is the phase difference between the oscillatory rods, similar in principle to freely-moving oscillators that can collectively swim [9–11]. We build on these past studies, which recognized the importance of phase in generating net motion, by examining the possible flow structures around a pair of rods undergoing prescribed oscillations.

The flow around rigid bodies undergoing oscillations is an important physical problem which offers fundamental insight into the basic underlying flow structure around more complex bodies. Organisms such as algae and crustaceans have numerous protruding body parts that often oscillate asynchronously [3, 12], which has inspired the design of microfluidic devices for mixing and pumping fluids [13]. While the bodies driving the motion in living and non-living systems are generally complicated by additional factors such as flexibility and inertia [14, 15], the resultant fluid-structure interactions yield a difference in phase which is key to generating flow. Our minimal experimental system is designed to isolate the key role of phase delay in order to examine its effect on the resultant flow. We employ methods to

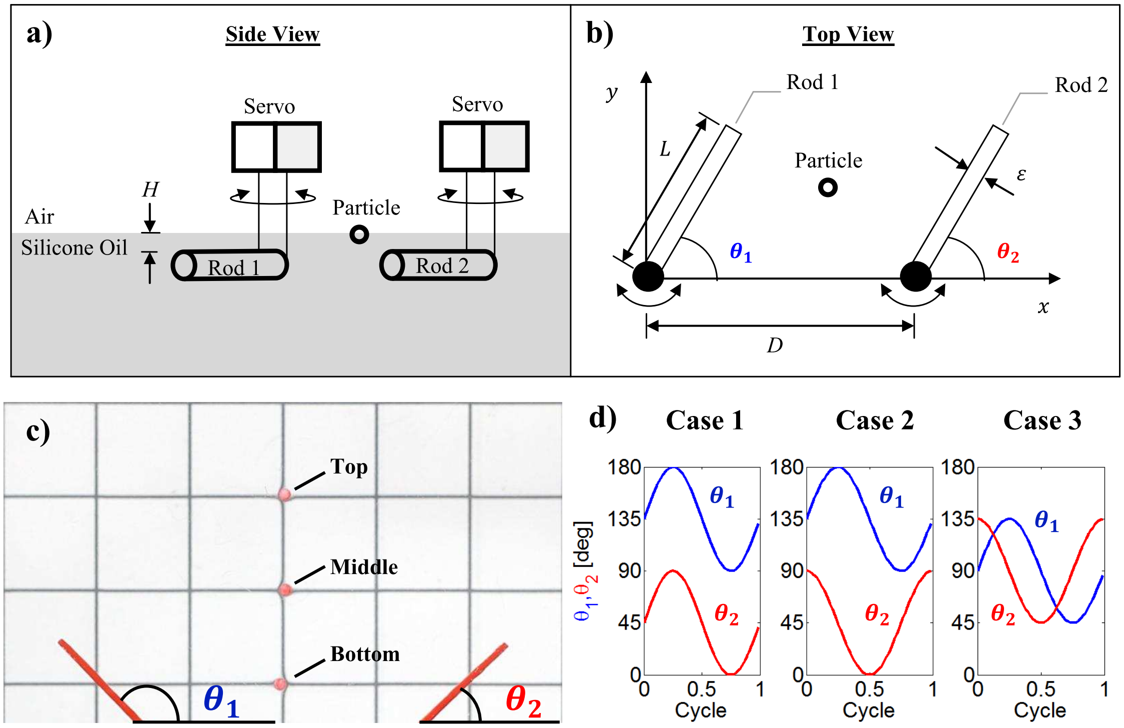

FIG. 1. Schematics of the experimental setup viewed from **(a)** the side and **(b)** the top. Servo-driven horizontal rods (Rods 1 and 2) of length L and diameter ϵ oscillate at distance H below the air-silicone oil interface. The two pivot points are separated by distance D. θ_1 and θ_2 are the angles of Rod 1 and Rod 2 with respect to the x-axis. (c) Three floating tracer particles (top, middle, and bottom) trace the fluid flow in the x-y plane. (d) Angular variations of the rods within one cycle for the three representative cases.

visualize and analyze the flow around a body completely immersed in fluid by considering one half of the body submerged beneath a free surface and exploiting reflective symmetry, which enables electric components to drive the body without getting them wet as done in our set up. The techniques are useful for studying flow around any symmetric body as commonly found in many systems, thus they are expected to apply to a broader class of problems having a plane of symmetry.

II. METHODS

The experimental system features a pair of servo-driven arms in silicone oil (Fig. 1a). Each arm (3D printed with ABS plastic) consists of a rigid horizontal rod (labeled Rod 1

Case	Description	ϕ (rad)	$\bar{\theta}_1$ (deg)	$\bar{\theta}_2$ (deg)	A (deg)
1	No phase delay	0	135	45	45
2	Phase delay, distinct mid-angles	$\pi/2$	135	45	45
3	Phase delay, same mid-angles	$\pi/2$	90	90	42

TABLE I. Median angle, phase difference, and amplitude for each case.

and Rod 2) of length $L = 40\,\mathrm{mm}$ and diameter $2\epsilon = 2\,\mathrm{mm}$, supported by a vertical rod of the same length and diameter 2.75 mm. The arms are dipped to a depth of $H = 5\,\mathrm{mm}$ below the surface of a large cylindrical bath (depth 115 mm and diameter 300 mm) of silicone oil (viscosity $\nu = 12500\,\mathrm{mm}^2/\mathrm{s}$ at room temperature).

The two arms are driven independently by servos (TowerPro SG90) to pivot around fixed vertical axes separated by a distance $D = 40\,\mathrm{mm}$ (Fig. 1b). The horizontal directions from one pivot along and across the line to the other pivot are denoted by x and y axes respectively. We set each rod i to oscillate periodically over time t such that it makes an angle θ_i with the x axis according to

$$\theta_1(t) = \bar{\theta}_1 + A\sin(\omega t), \tag{1}$$

$$\theta_2(t) = \bar{\theta}_2 + A\sin(\omega t + \phi). \tag{2}$$

The phase difference ϕ and the mid-angle $\bar{\theta}_i$ around which each rod oscillates have profound effects on the resultant flow, as investigated below in three representative cases (Table II and Fig. 1d). The amplitude is fixed to $A = 45°$, except in the final case where it is reduced slightly to avoid the rods from coming into contact. The angular frequency is fixed to $\omega = 0.115$ rad/s (oscillation period is $T = 2\pi/\omega = 54.6\,\mathrm{s}$) so that the Reynolds number $Re = \omega L^2/\nu = 0.015$ remains small.

Fluid flow on the surface is visualized with tracer particles (buoyant plastic spheres of diameter 2.75 mm). Their positions are recorded at five frames per second (Sony Alpha A6000 camera) and tracked using an open source tracking software (Tracker). Each experiment starts with three tracer particles located between the rods (Fig. 1c); they are labeled as the top particle (with initial coordinates $x = 20\,\mathrm{mm}$, $y = 60\,\mathrm{mm}$), middle particle ($x = 20\,\mathrm{mm}$, $y = 40\,\mathrm{mm}$), and bottom particle ($x = 20\,\mathrm{mm}$, $y = 20\,\mathrm{mm}$).

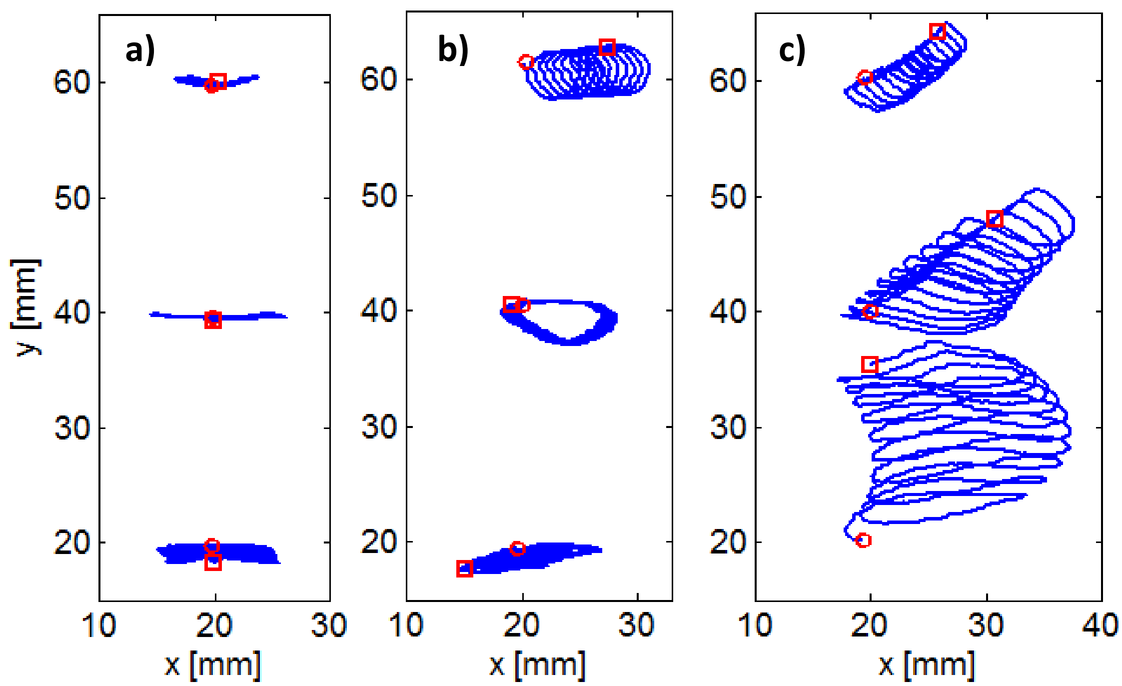

FIG. 2. Experimental trajectories of the three tracer particles for a duration of ten periodic cycles in (a) Case 1, (b) Case 2 and (c) Case 3. The initial and final positions are marked with a circle and square, respectively.

III. RESULTS

Trajectories of the three particles after ten periodic cycles are shown in Fig. 2. In Case 1 with no phase difference, each particle follows an almost linear path and then traces the same path back within every cycle (Movie 1) [16]. However, with a phase difference of a quarter period in Case 2, all three particles orbit counterclockwise (CCW) every cycle while the top and bottom particles drift away in opposite directions (Movie 2) [16]. Finally, with the two rods oscillating around the same mid-angle orientation in Case 3, all three particles follow a figure-of-8 pattern while drifting away from their initial position (Movie 3) [16]. These distinct trajectory patterns demonstrate that the phase difference and orientation of oscillatory rods have profound effects on the resultant flow.

The particle positions are sampled after each periodic cycle to show the net motion per cycle (Fig. 3). We performed each experimental case three times to verify repeatability. In Case 1 (Fig. 3a), no noticeable net motion is generated per cycle, drifting at most 1.5±0.3 mm after ten periodic cycles for the bottom particle. In Case 2 (Fig. 3b), significant net motion

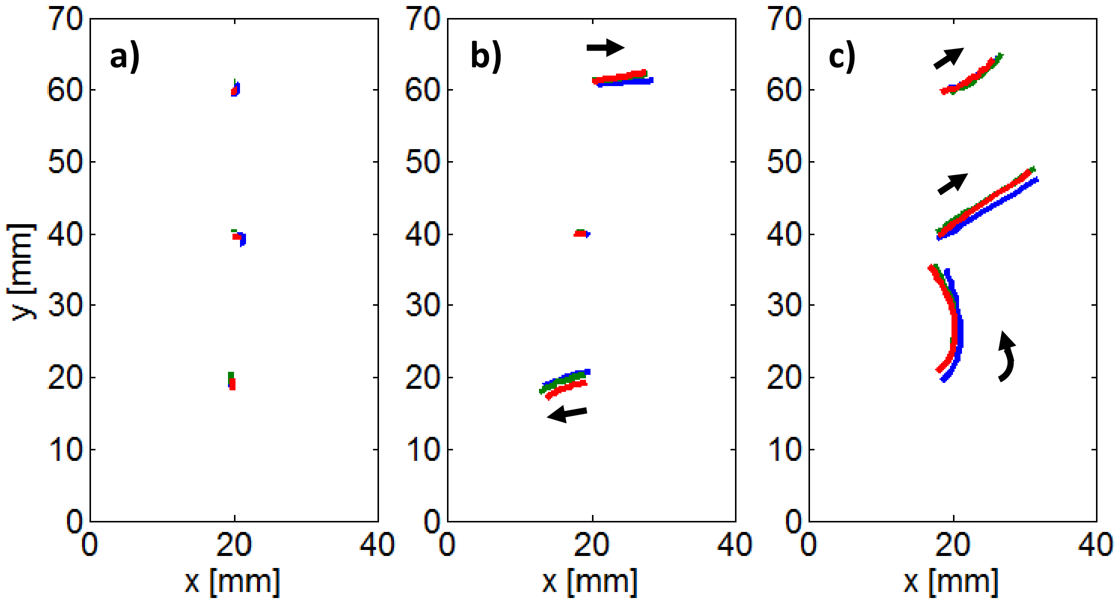

FIG. 3. Experimental trajectories of the three tracer particles sampled after each cycle in **(a)** Case 1, **(b)** Case 2 and **(c)** Case 3 for a duration of ten periodic cycles. For each case, three separate runs were repeated. Arrows point in the general direction of flow.

is generated for the top and bottom particle. The top particle drifted 7.4 ± 0.3 mm in the positive direction of the x-axis while the bottom particle drifted 4.9 ± 0.3 mm in the opposite direction. No noticeable net motion is generated for the middle particle. In Case 3 (Fig. 3c), all three particles generated considerable net motion. The top and middle particles drifted diagonally by 7.6 ± 0.4 mm and 13.9 ± 0.3 mm while the bottom particle drifted predominantly upward by 15.1 ± 0.5 mm after ten periodic cycles.

To gain further insights into the experiments, we simulated Stokes flow around the arms using the method of regularized Stokeslets [7]. Each arm is represented by 23 Stokeslets, 3 along the centerline of the vertical and 20 along the horizontal rod, such that the Stokeslets are equally spaced apart. The Stokeslet singularity is regularized using the commonly used 'blob' function $\phi_\delta(r) = 15\delta^4/8\pi(r^2 + \delta^2)^{7/2}$, where the blob size δ is set to half the radius ϵ of the rod. In order to impose the stress-free boundary condition at the free surface, we introduced image Stokeslets [17], reflections in the free surface shown in Fig. 4. This assumption is valid for sufficiently weak flow on the free surface such that the surface remains approximately flat. The wall and floor confining the flow are sufficiently far from the region of interest and thus neglected in the simulations. The strength of each Stokeslet is computed

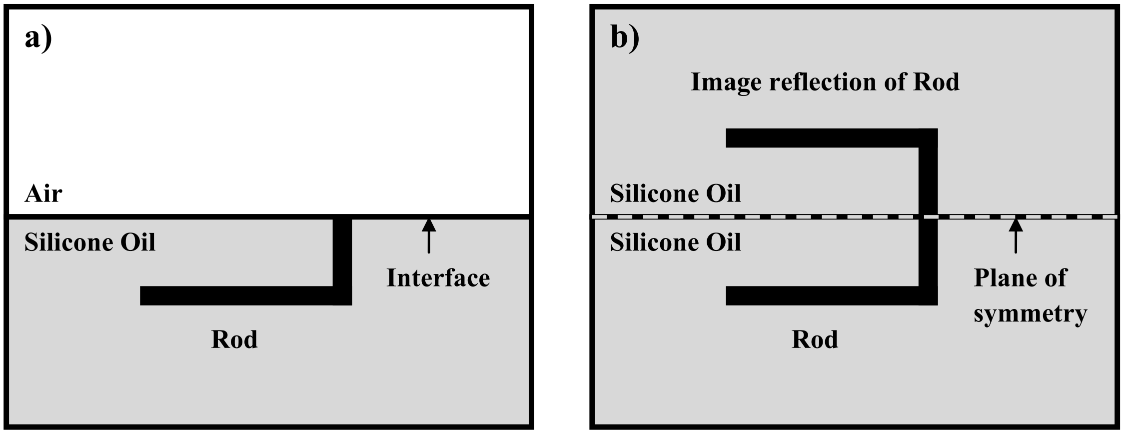

FIG. 4. **(a)** A side-view diagram of the rod submerged beneath an air-silicone oil interface. **(b)** A side-view diagram of a symmetric pair of rods completely immersed in silicone oil. The flow below the plane of symmetry is a reflection of that above the plane and is equivalent to the flow beneath the interface.

at each time step by prescribing the velocity of the rods as in the experiments. This enables prediction of the entire fluid flow field, and consequently the particle trajectory given any initial position. The particle positions are marched forward in time with 1000 time steps per cycle.

Simulated trajectories for the first periodic cycle are compared with the experimentally observed trajectories in Fig. 5, where the three trajectories in the middle column start with the same initial conditions as in the experiments. In Case 1, all simulated particles move in a line as observed in the experiment. In Case 2, all simulated particles orbit CCW as in the experiments. In Case 3, the top and middle particles orbit CCW whereas the bottom particle orbits CW, again in agreement with experiments. Furthermore, trajectories simulated away from the middle show a figure-of-8 pattern, consistent with those observed experimentally in Case 3 (Fig. 2*c*). Although the simulated orbits are slightly smaller than those observed in Case 2 and slightly larger in Case 3, the final positions are in reasonable agreement with experiments.

The long term behavior in Cases 2 and 3 observed in Fig. 3 is shown by the simulated displacement field after five periodic cycles (arrows in Fig. 6). For comparison we show the experimental data (circles) for particle positions sampled every five cycles over a duration of 30 cycles. In both cases, simulations show a swirling region in between the rods, consistent

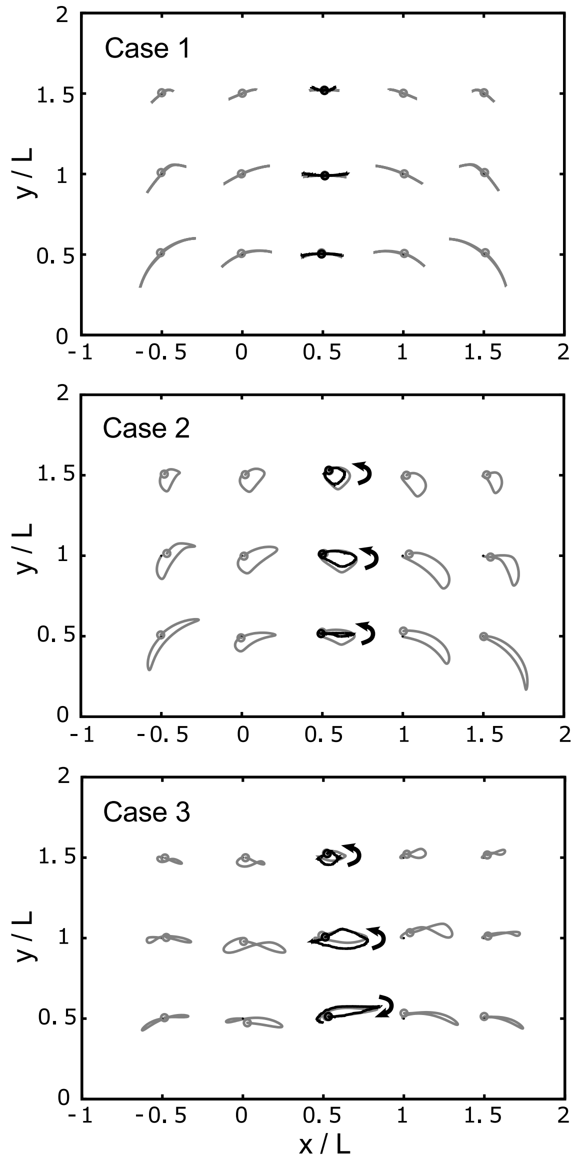

FIG. 5. Particle trajectories starting at different positions in Case 1 (top panel), Case 2 (middle panel) and Case 3 (bottom panel). Experimental data (black curves) are compared with simulations (grey curves) within one oscillatory cycle. Open circles represent final positions after one complete cycle. Arrows indicate the sense of rotation.

with the observed motion of the bottom particle following the swirl in the CCW sense. Simulations also show a large drifting region above the rods, consistent with the observed drift of the top particle in Case 2 and top and middle particles in Case 3. In between the swirling and drifting regions is a small stagnant region where the displacement arrows point in opposite directions and have relatively small magnitudes. The presence of this region is

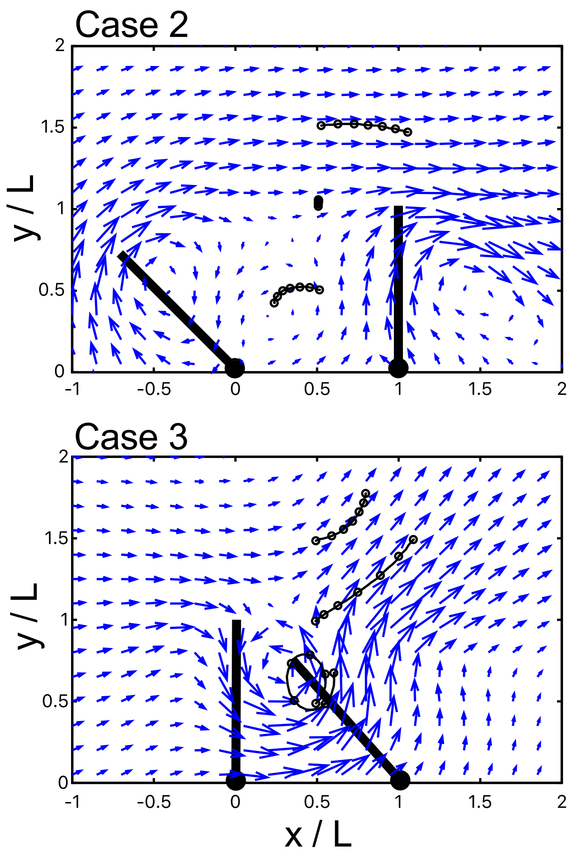

FIG. 6. Net motion of particle tracers in Case 2 (top panel) and Case 3 (bottom panel). Experimental data of particle positions sampled every periodic cycle are connected by black lines, with circle markers representing the positions every five cycles. Blue arrows indicate simulated displacements after five cycles. The black bars represent the initial configuration of the rods. Note that the tracers are above the plane of the rods and can appear to pass through them.

consistent with the long-term stagnant behavior of the middle particle in Case 2, though the center points of the stagnant and swirling regions do not exactly match those observed in the experiments. The formation of distinct flow regions and possible sources of discrepancy between the simulated and observed data are discussed below.

So far we have focused on the 2D flow in the plane of symmetry, where there is no velocity component in the direction normal to the plane. However, in a different plane parallel to the plane of symmetry, our simulations predict a 3D flow field in the bulk fluid. In the plane containing the rods, the displacement after one cycle has an upward or downward component as shown in the left column of Fig. 7. The right column shows that the vertical component is small compared to the total displacement, indicating that the displacement is

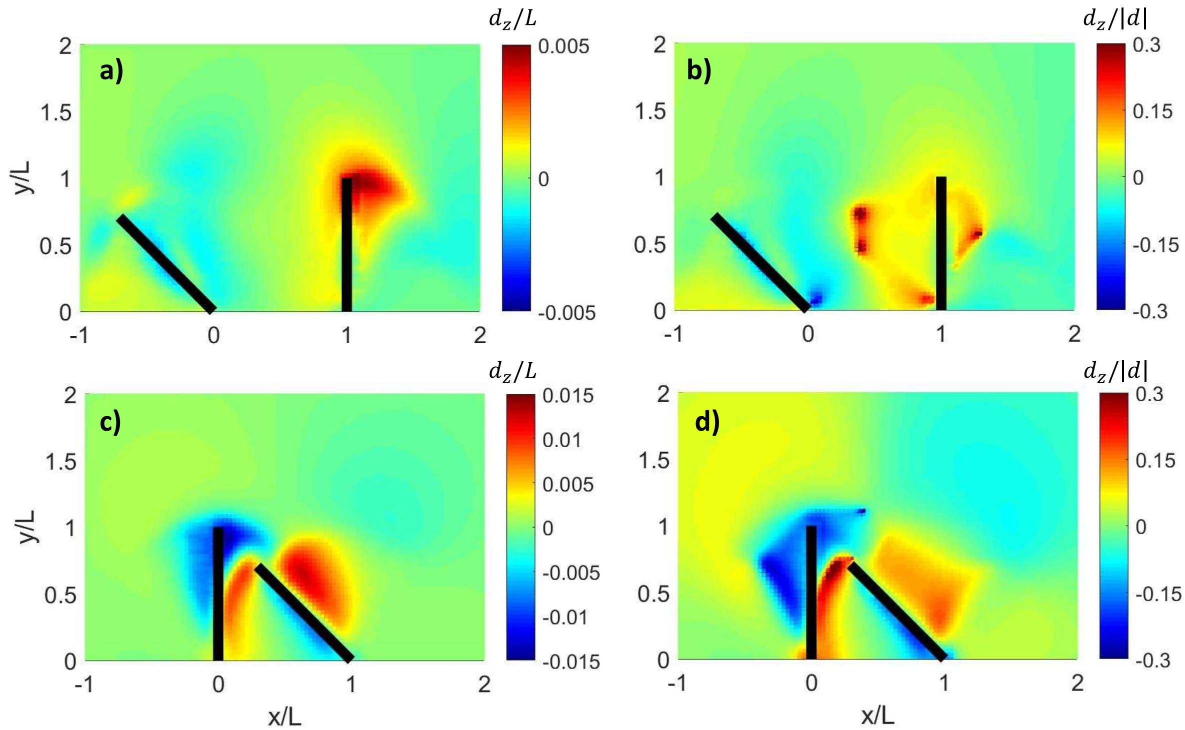

FIG. 7. Vertically upward component of the displacement field after one cycle at the plane of the rods, located at a depth z=-6 mm below the plane of symmetry. The vertical component d_z is scaled by **(a)** L or **(b)** $|d|$, the magnitude of the total displacement, in Case 2. **(c,d)** Corresponding results in Case 3. The black bars represent the initial configuration of the rods.

primarily horizontal. The horizontal displacement field is similar to Fig. 6 (not shown). In both Cases 2 and 3, the vertical displacement is most pronounced near the rods, implying that the fluid spirals up or down there. These results demonstrate that complex 3D flow structures can arise from interactions between oscillating rods and their reflected images.

We performed additional simulations to explore the dependence on various parameters, including the phase difference ϕ, amplitude A, and spacing distance D between the two pivot points. A measure of the fluid transport around the rods is given by the magnitude $|d|$ of the displacement of the top particle ($x/L = 0.5$, $y/L = 1.5$) after one cycle, which is plotted as a function of ϕ in Fig. 8a. The maximal displacement occurs at $\phi = \pm\pi/2$ in Case 2 but at a slightly different ϕ in Case 3. The displacement is primarily horizontal and can switch direction (Fig. 8b), with no net displacement generated at $\phi = 0$ and π as expected. In Fig. 8c and d, the net displacement increases as amplitude A increases and as the spacing D decreases. Note that we set the initial position to be half way between the

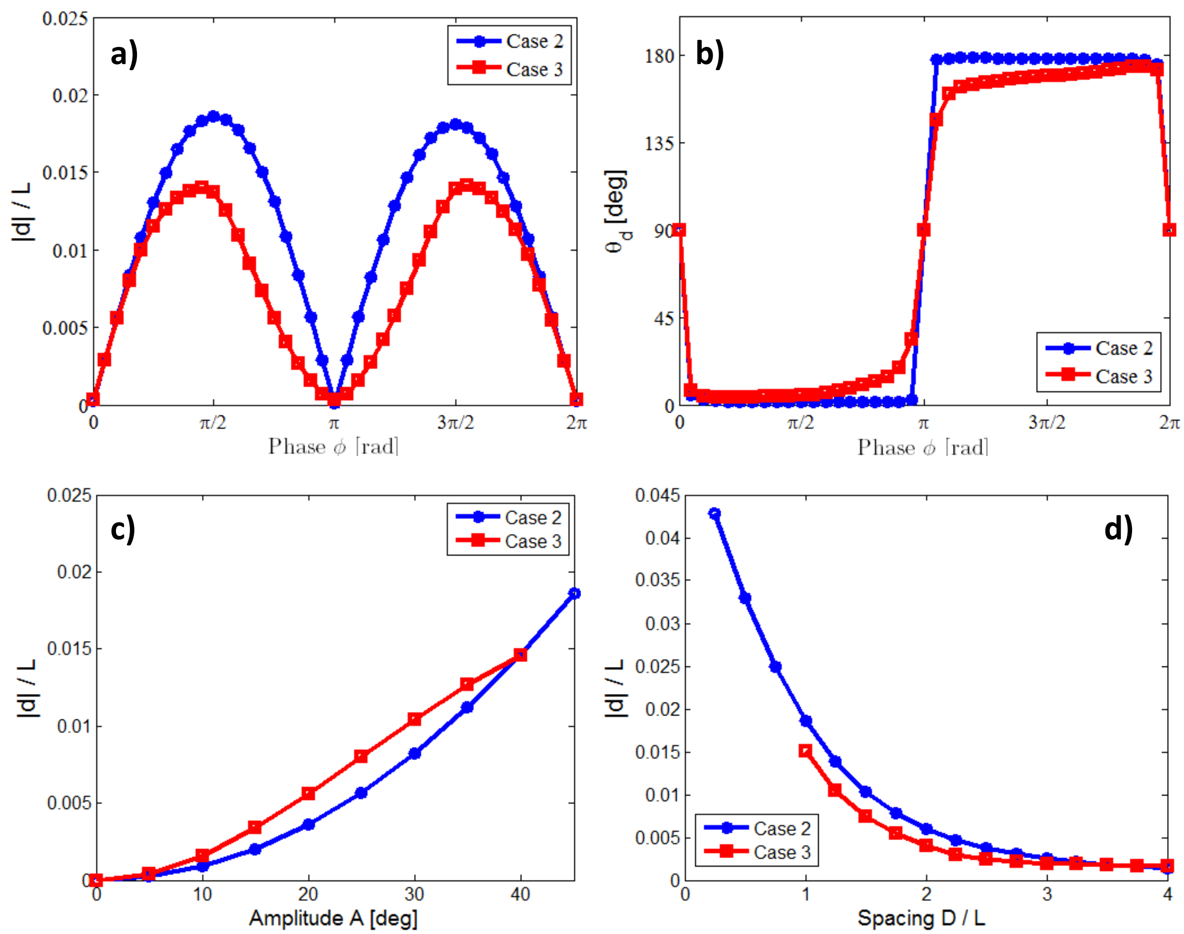

FIG. 8. Simulated displacements of the top particle (initially located at x/L = D/2, y/L = 1.5) after one cycle depending on **(a,b)** the phase difference ϕ, **(c)** amplitude A, and **(d)** distance D between the two pivot points. In **(b)** the displacement direction is measured by the angle θ_d it makes with the x axis. The angle θ_d switching from zero to π corresponds to reversal in the direction of displacement. The circle cursor is for Case 2 and the square cursor is for Case 3.

rods ($x/L = D/2$) and restricted the parameter range so as to prevent the two rods from coming into contact with each other. We also investigated the bottom and middle particles which showed similar trends.

IV. DISCUSSION

The direction of net flow in the drifting region outside the rods can be partly explained by considering the orientation of the rods at different stages within each cycle. At the critical instants when a rod attains maximal speed (see Fig. 1d and Movies 4 and 5) [16], the other rod is stagnant and drags the flow. This drag is greater when each rod moves to the left while the other stagnant rod is closer, compared to when each rod moves to the right while the other stagnant rod is further away, leading to a net rightward flow in the outer region. The flow is in the direction away from the rod that is delayed in phase. This is consistent with the direction of motion of multi-legged swimmers whose legs oscillate with a phase delay closer to the front end of their body [11].

Why does the region in between the rods swirl in the CCW sense? Let us first consider tracer particles initially above the second pivot point, that is, in the vicinity along Rod 2 in Case 2. The particles predominantly follow the direction of motion of Rod 2, with a slight modification due to the motion of the more distant Rod 1 (Movie 4) [16]. This modification drives the particles downwards when Rod 1 has a downward moving component but drives the particles upwards by a greater amount when Rod 1 has an upward component, when Rod 2 is further away from the particles. This leads to an upward drift above the second pivot point. By a similar argument, we expect a downward drift above the first pivot point. By continuity we expect a CCW swirl in the region in between the rods. The larger scale swirls may be able to rotate large objects of similar size which may be useful for organisms and bioinspired robots to probe objects in their environment.

There is a few possible sources of discrepancy between the experiments and simulations. We initially placed the rods at the air-liquid interface but that resulted in an unsatisfactory comparison between the simulation and experiment due to noticeable surface deformation, with the motion of each rod causing the surface to slightly rise ahead and dip behind it. By lowering the rods below the interface, we were able to keep the surface almost undeformed and get a better agreement. Nevertheless, a very minor deformation at the interface may have contributed to the slight discrepancy between the experiments and simulations. We chose not to lower the rods deeper into the liquid because that would result in a weaker flow on the surface and increased effects of the floor. The silicone oil is bounded by the wall and floor of the container which is not accounted for in the model. While the model does not capture all aspects of the flow in quantitative detail, it nevertheless provides results consistent with the main experimental findings. This demonstrates that any Stokes flow containing a plane of symmetry could be studied theoretically and experimentally by exploiting the symmetry and considering one half of the region as done in our model and experiments. Thus our approach could be applied to a broader class of Stokes flow problems featuring a plane of symmetry.

There are numerous important implications of flows driven by oscillatory motion at low Re, as commonly encountered in nature, for instance, in biological systems. A specific example is the asynchronous beating of a pair of flagella and the sharp turns associated with swimming cells [3]. If the phase is delayed in the left flagellum compared to the right such as in Case 2, we expect outer flow circulation to the right, thus driving the cell to turn CCW. The flexibility of flagella may reinforce or counter the flow. In other situations, slender bodies could oscillate passively in response to an external periodic force, and the oscillations may not be in phase if the bodies respond differently to the force. The different responses could be exploited to generate flow at low Reynolds number in numerous applications, for instant for pumping and mixing fluids in microfluidic devices. The basic underlying structure of the resultant flow should have drifting and swirling regions as presented here.

In conclusion, a complex flow field can be obtained in a viscous fluid by the asynchronous oscillation of two rigid rods. The rich flow field consists of small orbital motion every periodic cycle and larger drifting or swirling motion after many cycles. Suspended particles can drift in different directions depending on their initial positions. The experiments agree well with simulations based on the method of regularized Stokeslets. The simulations show that fluid is most transported with an optimal phase difference of a quarter period, and moreover, reveal complex 3D flow structures away from the plane of symmetry. The motion arises generally for any phase difference, except in the special case of oscillations that are completely in-phase or anti-phase. Even a small difference in phase should generate flow every cycle, thus the phase-induced flow is expected to arise ubiquitously in a variety of fluids driven by a system of oscillatory body parts, as commonly encountered in biological physics and technological applications.

ACKNOWLEDGMENTS

This work was supported by NSF (CBET-1603929) and ARO (W911NF-15-1-0608).

[1] G. I. Taylor, "Low Reynolds number flows," National Committee for Fluid Mechanics Films (1967).

[2] E. M. Purcell, “Life at low Reynolds number,” Am. J. Phys. **45**, 3 (1977).

[3] M. Polin, I. Tuval, K. Drescher, J. P. Gollub, and R. E. Goldstein, “Chlamydomonas swims with two “gears” in a eukaryotic version of run-and-tumble locomotion,” Science **325**, 487–490 (2009).

[4] J. S. Guasto, K. A. Johnson, and J. P. Gollub, “Oscillatory flows induced by microorganisms swimming in two dimensions,” Phys. Rev. Lett. **105**, 168102 (2010).

[5] E. Lauga and T. R. Powers, “The hydrodynamics of swimming microorganisms,” Rep. Prog. Phys. **72**, 096601 (2009).

[6] M. Peplow, “March of the machines,” Nature **525**, 18 (2015).

[7] R. Cortez, “The method of regularized Stokeslets,” SIAM J. Sci. Comput. **23**, 1204–1225 (2001).

[8] E. L. Bouzarth, A. Brooks, R. Camassa, H. Jing, T. J. Leiterman, R. M. McLaughlin, R. Superfine, J. Toledo, and L. Vicci, “Epicyclic orbits in a viscous fluid about a precessing rod: Theory and experiments at the micro- and macro-scales,” Phys. Rev. E **76**, 016313 (2007).

[9] G. P. Alexander and J. M. Yeomans, “Dumb-bell swimmers,” Europhys. Lett. **83**, 34006 (2008).

[10] E. Lauga and D. Bartolo, “No many-scallop theorem: Collective locomotion of reciprocal swimmers,” Phys. Rev. E **78**, 030901 (2008).

[11] D. Takagi, “Swimming with stiff legs at low Reynolds number,” Phys. Rev. E **92**, 023020 (2015).

[12] P. H. Lenz, D. Takagi, and D. K. Hartline, “Choreographed swimming of copepod nauplii,” J. R. Soc. Interface **12**, 20150776 (2015).

[13] S. N. Khaderi, J. M. J. den Toonder, and P. R. Onck, “Fluid flow due to collective non-reciprocal motion of symmetrically-beating artificial cilia,” Biomicrofluidics **6**, 014106 (2012).

[14] M. J. Shelley and J. Zhang, “Flapping and bending bodies interacting with fluid flows,” Annu. Rev. Fluid Mech. **43**, 449–465 (2011).

[15] C. Zhang, R. D. Guy, B. Mulloney, Q. Zhang, and T. J. Lewis, “Neural mechanism of optimal limb coordination in crustacean swimming,” Proc. Natl. Acad. Sci. **111**, 13840 (2014).

[16] See Supplemental Material at [URL] for the movies of experiments and simulations.

[17] J. Blake, “On the movement of mucus in the lung,” J. Biomech. **8**, 179–190 (1975).